Crystal field splitting and magnetic behavior of Nd_2BaCuO_5 single crystals

R. Sáez Puche, E. Climent, and J. Romero de Paz

Departamento de Química Inorgánica I, Facultad de Ciencias Químicas, Universidad Complutense de Madrid, 28040 Madrid, Spain

J. L. Martínez, M. A. Monge, and C. Cascales

Instituto de Ciencia de Materiales de Madrid, Consejo Superior de Investigaciones Científicas, Cantoblanco, 28049 Madrid, Spain
(Received 28 June 2004; published 6 January 2005)

Single crystals of Nd_2BaCuO_5 oxide have been prepared starting from the powder oxide, and x-ray structural determination and magnetic studies have been carried out. Nd_2BaCuO_5 crystallizes with tetragonal symmetry, space group $P4/mbm$. The temperature dependence of the magnetic susceptibility measured along the c axis shows a net maximum at 7.5 K, indicative of the presence of an antiferromagnetic ordering below that temperature. This behavior has been confirmed by specific heat measurements, which show a λ transition at 7.8 K. However, the magnetic susceptibility measured along the a axis does not show any maximum. This anisotropy has been explained as the result of the crystal field effect associated with the Nd^{3+} ion, by means of the determination of a consistent set of energy levels for the Nd_2BaCuO_5 oxide and the calculation of the paramagnetic susceptibilities according to the Van Vleck formalism. The rather low antiferromagnetically ordered magnetic moment of the Nd^{3+} ion, $0.81\mu_B$, is explained taking into account the calculated anisotropic g values of the crystal ground term of the Nd^{3+} ion.

I. INTRODUCTION

Oxides with the general formula R_2BaCuO_5, where R stands for rare earth, present two different structural types depending on the size of the R ion. Most of these oxides with R going from samarium to lutetium, including yttrium, crystallize with the so-called Sm_2BaCuO_5 structure type, showing orthorhombic symmetry, space group $Pnma$,[1] whereas the oxides with the lighter rare earths, i.e., lanthanum, praseodymium, and neodymium, crystallize with the Nd_2BaPtO_5 structure type with tetragonal symmetry, space group $P4/mbm$.[2] This structure can be described as formed by square planar $[CuO_4]$ units, which are isolated from each other forming a quasibidimensional arrangement, as can be observed in Fig. 1. These units are connected to one another by sharing an edge with a bicapped tetragonal prism $[BaO_{10}]$ in the ab plane. The R^{3+} ion is situated in a bicapped trigonal prism $[RO_8]$ sharing faces to form R_2O_5 layers that run parallel to the c axis of the structure.

A great number of papers have been devoted to the study of the magnetic and optical properties of the $Pnma$ R_2BaCuO_5 oxides, also known as green phases (see Refs. 3–5 and references therein), but knowledge about the $P4/mbm$ oxides is very scarce and, as far we know, only a few papers have been published concerning them. In this sense, it has been reported that La_2BaCuO_5 oxide behaves as ferromagnetic with a Curie temperature (T_C) of 5.7 K.[6] This is a rather unusual behavior among the copper oxides because most of the known cuprates of formula R_2BaCuO_5 have antiferromagnetic ground states. For this reason, the characteristic ferromagnetic behavior of La_2BaCuO_5 drew some interesting theoretical studies. Masuda *et al.*[7] reported from electron spin resonance measurements the relationships between the ferromagnetic and crystal structures of this compound. Feldkemper *et al.*[8] showed the existence of two main

different pathways through which the magnetic interactions take place. The first one involves half-filled $d_{x^2-y^2}$ and filled d_{z^2} orbitals of the nearest-neighbor Cu^{2+} atoms in the ab plane of the structure and, according to the Goodenough-Kanamori-Anderson (GKA) rules,[9] the interaction is predicted to be ferromagnetic. However, the second one takes place along the [001] direction and leads to an antiferromagnetic coupling. Since the interlayer Cu-Cu distance of 5.82 Å is larger than 4.82 Å found in the ab plane, this justifies the predominantly ferromagnetic ordering reported for the La_2BaCuO_5 oxide.

The substitution of the diamagnetic La^{3+} ion by Pr^{3+} and Nd^{3+} ions gives rise to important changes in the magnetic behavior of the isostructural Pr_2BaCuO_5 and Nd_2BaCuO_5 oxides. The Pr_2BaCuO_5 oxide, prepared in our research group, shows a ferromagnetic behavior with a $T_C = 15$ K.[10] Concerning Nd_2BaCuO_5 only three papers,[11–13] as far we know, are devoted to the magnetic properties of this oxide, which presents an antiferromagnetic behavior with a Néel temperature (T_N) of 7.5 K. Hence, substituting a different paramagnetic rare earth for lanthanum can affect the ferromagnetism in La_2BaCuO_5 oxide. The studies reported previously reveal that neodymium destroys the ferromagnetic ordering while the nonmagnetic Eu^{3+} does not affect the magnetic interaction.[14] Very recently Nozaki *et al.* have reported a systematic study of the lanthanum substitution effect by other paramagnetic lanthanide cations on the ferromagnetism in La_2BaCuO_5 oxide.[15]

Our goal with this work is to grow single crystals of the Nd_2BaCuO_5 oxide, in order to have a better understanding of the nature of the magnetic interactions and the mechanism through which they take place in this complex oxide. For this purpose magnetic studies on single crystals and calorimetric measurements have been performed.
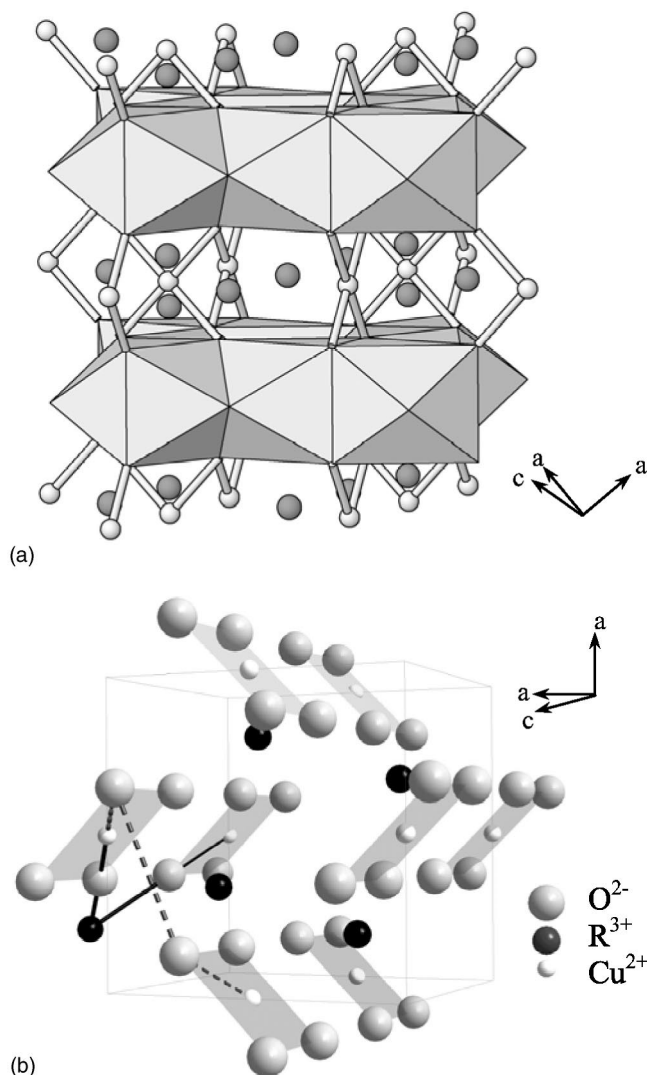
FIG. 1. Perspective views of Nd_2BaPtO_5-type structure of the so-called brown phases R_2BaCuO_5 (R: La or Nd), showing (a) the RO_8 layers (gray polyhedra), square-planar CuO_4 (stick and balls), and barium atoms (dark gray circles); and (b) the different magnetic interaction pathways as dashed and bold lines (see text).

II. EXPERIMENTAL DETAILS

Nd_2BaCuO_5 oxide was prepared first as a powder sample by heating the stoichiometric amounts of Nd_2O_3, $BaCO_3$, and CuO at 950 °C for 12 h in air. After grinding to homogenize and enhance the reaction rate, the sample was fired at 1000 °C for 24 h yielding a brown powdered Nd_2BaCuO_5 oxide. On heating the powdered Nd_2BaCuO_5 sample up to 1450 °C in a platinum crucible the sample melts. Then, the temperature was decreased at a rate of 3 °C/h down to 1200 °C, and then at 10 °C/h down to 1000 °C. After switching off the furnace and to cooling room temperature, black crystals of prismatic shape were obtained. See Fig. 2.

A black prismatic single crystal of dimensions $0.16 \times 0.06 \times 0.06$ mm³ was mounted on a Brucker-Siemens Smart charge-coupled device diffractometer equipped with a normal focus, 3 kW sealed tube. Data were collected over the
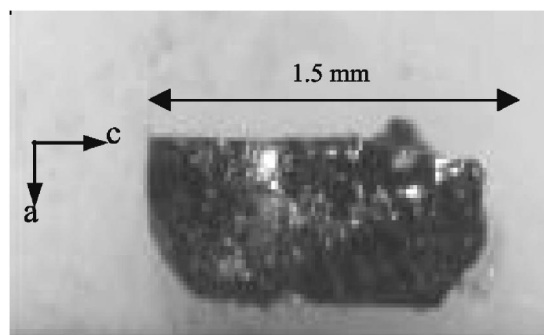
FIG. 2. Prismatic single crystal of Nd_2BaCuO_5 oxide with the largest dimension parallel to the c axis of the structure.

full sphere of the reciprocal space by a combination of four frame sets. The θ range was 3.49° to 28.86°. The crystal to detector distance was 5.02 cm. The unit cell dimensions were determined and refined by least-squares fit of all collected reflections. Each exposure of 20 s covered 0.3° in ω. The first 50 frames were recollected at the end of the data collection to monitor crystal decay. The intensities were corrected for Lorentz and polarization effects. Scattering factors for neutral atoms were taken from the *International Tables for X-Ray Crystallography*. The structure was solved by Multan and Fourier methods. Full matrix least-squares refinement was carried out minimizing $w(F_0^2 - F_c^2)^2$. Refinement of the electron density at the $2d$ site showed that that position was shared by Cu and Pt atoms, with population factors of 0.816(1) and 0.184(1), respectively. Most of the calculations were carried out with shelxtl for structure solution and refinements.[16] A summary of the fundamental crystal and refinement data is given in Table I.

Magnetic susceptibility and magnetization measurements were performed in a Quantum Design XL-MPMS superconducting quantum interference device magnetometer at different magnetic fields in the temperature range 2–300 K. Anisotropic magnetic susceptibility measurements were taken in a single crystal of dimensions $2.0 \times 0.5 \times 0.5$ mm³, where the c axis is aligned to the largest dimension of the single crystal, as can be observed in Fig. 2. After taking the so-called parallel susceptibility $\chi_\parallel$, the crystal was rotated 90° around the a axis and the perpendicular susceptibility $\chi_\perp$ was measured, which is coincident with the ab plane of the structure according to the tetragonal symmetry of the structure.

The specific heat was measured by the heat phase-relaxation method in a Quantum Design PPMS equipment. The temperature range was from 1.7 to 300 K and we used magnetic fields up to 9 T. A few prismatic single crystals (approximately 15 mg) were attached to a sapphire platform by a small amount of Apiezon N grease. The added heat capacity was measured in a separated run and subtracted from the sample data.

III. RESULTS AND DISCUSSION

A. Structure refinement

Atomic parameters and interatomic distances and angles are shown in Tables II and III, respectively. Regarding the

TABLE I. Crystal data and structure refinement for $Nd_2BaCu_{0.82}Pt_{0.18}O_5$.

Empirical formula	$Nd_2BaCu_{0.82}Pt_{0.18}O_5$
Formula weight	593.56
Temperature	296(2) K
Wavelength	0.71073 Å
Crystal system	Tetragonal
Space group	$P4/mbm$
Unit cell dimensions	$a = 6.709(2)$Å
	$b = 6.709(2)$Å
	$c = 5.835(3)$Å
Volume, Z	262.68(17)Å^3, 2
Density (calculated)	4.833 mg/m^3
Absorption coefficient	28.626 mm^{-1}
$F(000)$	323
Crystal size	$0.16 \times 0.06 \times 0.06$ mm^3
θ range for data collection	3.49°–28.86°
Index ranges	$-9 < h < 8, -8 < k < 8, -7 < l < 7$
Reflections collected	2157
Independent reflections	$208[R(int) = 0.0383]$
Completeness to $\theta = 28.86°$	98.6%
Absorption correction	Semiempirical from equivalents
Max. and min. transmission	0.2785 and 0.0916
Refinement method	Fullmatrix leastsquares on F^2
Data/restraints/parameters	208/0/20
Goodness of fit on F^2	1.244
Final R indices $[I > 2\sigma(I)]$	$R1 = 0.0273, wR2 = 0.0567$
R indices (all data)	$R1 = 0.0293, wR2 = 0.0575$
Extinction coefficient	0.0107(10)

oxygen stoichiometry we have confirmed that no oxygen vacancies are present in the structure and refinements of the population factor at the Cu position yielded a composition of the crystals of $Nd_2BaCu_{0.816}Pt_{0.184}O_5$. It is known that the structure can be depicted as formed by layers of NdO_8 polyhedra sharing faces, connected via Cu square planes. As a consequence of this arrangement the shortest Nd-Nd distance takes the value of 3.30 Å. On the other hand, the intralayer Cu-Cu distance is 4.74 Å and the interlayer Cu-Cu one is 5.83 Å. As can be observed in Table III, the isolated square-planar $[CuO_4]$ units present four equal Cu-O distances but

TABLE II. Atomic coordinates and equivalent isotropic displacement parameters at room temperature for $Nd_2BaCu_{0.82}Pt_{0.18}O_5$ oxide. U(eq) is defined as one-third of the trace of the orthogonalized U^{ij} tensor.

Atom	Site	x	y	z	U(eq) (Å^2)
Nd(1)	4h	0.1740(1)	0.6740(1)	0.5	0.004(1)
Ba(2)	2a	0	1	0	0.007(1)
Cu(3)/Pt(1)	2d	0	0.5	0	0.004(1)
O(1)	8k	0.1395(8)	0.3605(8)	0.2446(12)	0.008(2)
O(2)	2b	0	1	0.5	0.007(3)

the two different planar angles reveal a distortion. Barium atoms are ten-coordinated and occupy the bicapped tetragonal prismatic holes that appear between each two NdO_8 layers and two CuO_4 square planes. See Fig 1(a).

B. Magnetic measurements

Magnetic susceptibility data obtained for a powdered Nd_2BaCuO_5 sample show a Curie-Weiss behavior over a wide temperature range 300–20 K and the obtained magnetic moment of $4.36\mu_B$ agrees with the calculated one taking the Nd^{3+} and Cu^{2+} contributions according to $\sqrt{\mu_{Nd^{3+}}^2 + \mu_{Cu^{2+}}^2}$ (Fig. 3). It is worth noting that although a negative Weiss constant (ϑ) has been obtained, -17 K, it is not possible to infer an antiferromagnetic behavior because in some cases it has been demonstrated that the negative value of the Weiss constant can be certainly assigned to the crystal field effect of the rare earth without claiming the onset of any antiferromagnetic interactions.[17] Moreover, the absence of the characteristic maximum ascribed to an antiferromagnetic behavior down to 2 K in the temperature dependence of the magnetic susceptibility, Fig. 3, deserves a further and more detailed study of the magnetic properties of this Nd_2BaCuO_5 oxide, described as antiferromagnetic,[13] as was mentioned

TABLE III. Interatomic lengths (Å) and main angles (deg) of NdO_8, BaO_{10} and CuO_4 polyhedra in $Nd_2BaCu_{0.82}Pt_{0.18}O_5$ oxide.

NdO_8	BaO_{10}	CuO_4
Nd(1)-O(1) 2.314(7) ($\times 2$)	Ba(2)-O(2) 2.918(1) ($\times 2$)	Cu(3)-O(1) 1.947(7) ($\times 4$)
Nd(1)-O(2) 2.480(1) ($\times 2$)	Ba(2)-O(1) 2.961(4) ($\times 8$)	
Nd(1)-O(1) 2.588(6) ($\times 4$)		
O(1)-Nd(1)-O(1) 80.2(4)		O(1)-Cu(3)-O(1) 85.7(4) ($\times 2$)
O(1)-Nd(1)-O(1) 61.5(3) ($\times 2$)		O(1)-Cu(3)-O(1) 94.3(4) ($\times 2$)
O(1)-Nd(1)-O(1) 100.7(2) ($\times 2$)		O(1)-Cu(3)-O(1) 180.0 ($\times 2$)
O(1)-Nd(1)-O(1) 70.3(2) ($\times 2$)		
O(1)-Nd(1)-O(1) 149.18(15) ($\times 4$)		
O(1)-Nd(1)-O(1) 96.7(3) ($\times 4$)		
O(2)-Nd(1)-O(2) 146.16(3)		

earlier. In order to better understand the magnetic properties of this compound, anisotropic properties of single crystals should be studied.

Figure 4 shows the temperature dependence of the anisotropic magnetic susceptibility $\chi_\parallel$ and $\chi_\perp$ for a single crystal. As in the case of the powdered sample, the susceptibility obeys a Curie-Weiss law in a wide range of temperatures, 30–300 K, but the obtained magnetic moment for the $\chi_\parallel$ data, which takes the value of $4.25\mu_B$, is slightly higher than the corresponding value for $\chi_\perp$, which is $4.03\mu_B$. The average moment obtained from the representation of the average susceptibility, calculated by the formula $\chi_{av} = 2/3\chi_\parallel + 1/3\chi_\perp$, takes the value of $4.20\mu_B$ so it agrees well with that obtained for the powdered sample. The higher value of $\chi_\perp$ compared to $\chi_\parallel$ agrees with the absence of any maximum in the magnetic susceptibility data obtained from the powder (which is equivalent to χ_{av}) mentioned earlier.

As it can be observed in Fig. 4, $\chi_\parallel$ reaches a maximum at 7.5 K which corresponds to the onset of an antiferromagnetic transition. It is noted that the doping of the Cu^{2+} sublattice with Pt^{2+} during the crystal growth process does not affect

T_N, which is coincident with data reported earlier by Klimin *et al.* from optical spectroscopy studies.[11] As deduced from molecular field theory, $\chi_\parallel$ decreases below T_N with decreasing temperature, but $\chi_\perp$ shows a very different behavior if it is compared with that expected for typical antiferromagnetic materials. That is, $\chi_\perp$ increases with decreasing temperatures and it can be observed, as a special characteristic of this compound, that $\chi_\parallel$ and $\chi_\perp$ take different values even above the T_N. It can be observed that in the whole range of temperatures the $\chi_\perp$ values are higher than the $\chi_\parallel$ ones. This deviation from the classical molecular field approach can be explained by considering the crystal field effect of the Nd^{3+} ion, which is occupying a C_{2v} point symmetry site. The theoretical simulation of the magnetic susceptibility is reported in this paper.

The origin of this antiferromagnetic behavior can be explained using the classical GKA rules. These rules cannot be applied in a simple manner, it is necessary to analyze the different superexchange pathways through the magnetic interactions taking place. As summarized in the Introduction, there are two possible superexchange mechanisms which are
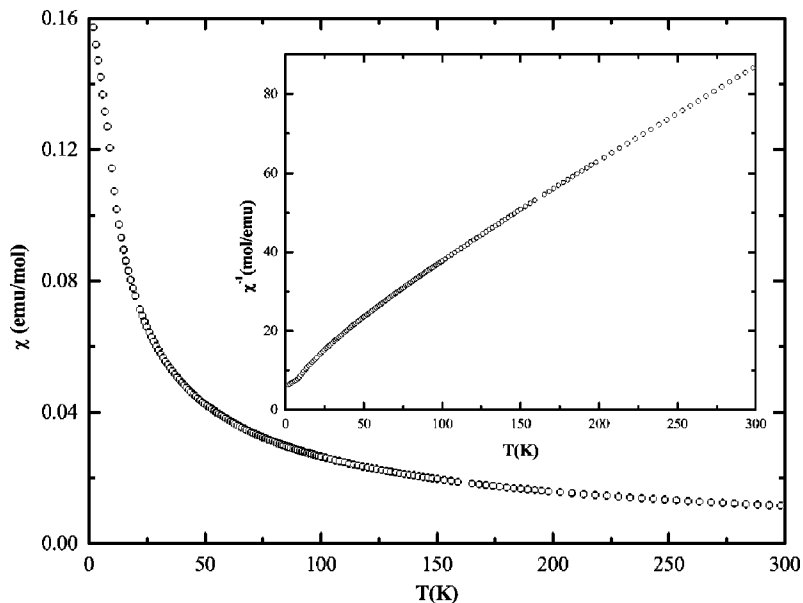
FIG. 3. Magnetic susceptibility versus temperature for powdered Nd_2BaCuO_5 oxide. The inset shows the temperature dependence of the inverse magnetic susceptibility.
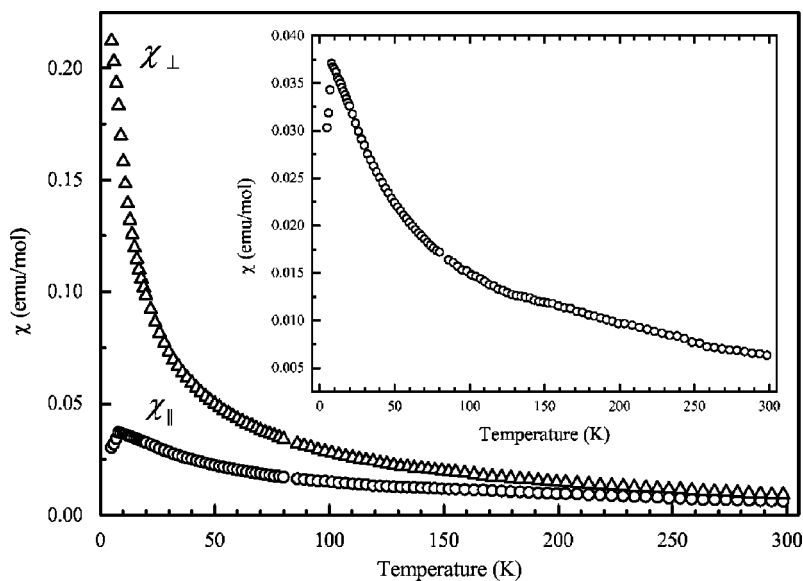
FIG. 4. Magnetic susceptibility versus temperature for single-crystal Nd_2BaCuO_5 oxide. The triangles correspond to the magnetic susceptibility measured along the a axis ($\chi_\perp$), and the circles correspond to the magnetic susceptibility measured along the c axis ($\chi_\parallel$) which is more clearly shown in the inset.

shown in Fig. 1(b). The first one (dashed line) is of the type Cu-O(1)-O(1)-Cu and takes place between copper atoms within the ab plane, and according to the GKA rules is predicted to be ferromagnetic. The second one (bold line) is of the type Cu-O(1)-R-O(1)-Cu, takes place along the c axis involving the copper atoms' half-filled $d_{x^2-y^2}$ orbitals, and according to the GKA rules will produce an antiferromagnetic interaction. So the presence of the paramagnetic Nd^{3+} instead of the diamagnetic La^{3+} should explain the rather different magnetic behavior between antiferromagnetic Nd_2BaCuO_5 oxide and ferromagnetic La_2BaCuO_5 oxide. Although the Cu-Cu distances within the ab plane are shorter than the Cu-Cu interlayer distances, the Cu-O(1)-Nd-O(1)-Cu pathway along the c axis becomes predominant because of the Cu-O(1)-Nd interactions, which are strongly favored by the angle and distance associated with this interaction, 172.9(4)° and 4.26 Å, respectively, yielding a very important overlap of the orbitals. This could explain why the partial substitution of Cu^{2+} by Pt^{2+} does not affect the magnetic behavior of the Nd_2BaCuO_5 oxide, since it is mainly controlled by the mentioned Cu-O(1)-Nd interactions. It is worth nothing that in the case of the isostructural $LaEuBaCuO_5$ oxide, the ferromagnetic character remains because the nonmagnetic $^7F_0$ ground state of Eu^{3+} should be populated at 5 K, which corresponds to the T_C of this oxide, and the interlayer Cu-O-La/Eu-O-Cu pathway is analogous to the case La_2BaCuO_5, so the substitution of half of the La^{3+} by the nonmagnetic Eu^{3+} does not affect the sign of the interaction.[14]

On the other hand, the magnetic structure determined from powder neutron diffraction data[13] confirms the model proposed above, where the copper moments are antiferromagnetically aligned along the c axis, forming a simple antiferromagnetic lattice, while the Nd moments are lying in the ab plane. However, we note the onset of just one magnetic reflection and the very weak increase of the intensity of a few of the nuclear reflections in the ordered state below T_N. Although the propagation vector $\left(00\frac{1}{2}\right)$ appears to fit this magnetic reflection, the very weak contribution arising from the magnetic moments yields a high degree of uncertainty in the determination of the magnetic structure.

C. Specific heat measurements

In order to investigate the antiferromagnetic transition in more detail, specific heat measurements have been performed at different temperatures and magnetic field strengths. Figure 5 shows the presence of a λ-type transition at 7.8 K when the magnetic field is 0 Oe, which corresponds to the antiferromagnetic ordering detected at the same temperature from the magnetic susceptibility measurements. By increasing the external magnetic field the temperature of the λ-type transition decreases gradually, reaching a value of 7 K when the field is 9 T (see inset of Fig. 5). In the same manner the intensity of the λ peak decreases. This is the typical perturbation of the ordered state by increasing the external field.

The total measured specific heat (C) consists of the magnetic (C_{mag}), electronic (C_e), and lattice (C_l) contributions, so to calculate the magnetic contribution to the specific heat it is necessary to discount the electronic and lattice contributions from the total specific heat. The calculation of these two latter contributions has been done using a polynomial function of the temperature such as $F(T)=A+BT+CT^2+DT^3$. The constants were determined by fitting the polynomial function to the experimental specific heat obtained between 10 and 50 K. The calculated data are plotted in Fig. 5 as a solid line and the magnetic specific heat is obtained by subtracting these calculated values from the total experimental specific heat. The evolution of this C_{mag} value against the temperature is plotted in Fig. 6 and it can be observed that the C_{mag} value remains almost constant in the temperature range 50–15 K. By contrast, at 10 K the onset of a sharp increase can be visualized, reaching a net maximum at 7.8 K, which corresponds to a T_N that fully agrees with the one estimated from the magnetic susceptibility measurements.

The magnetic entropy (S_{mag}) has been calculated by integrating C_{mag} as a function of the temperature according to
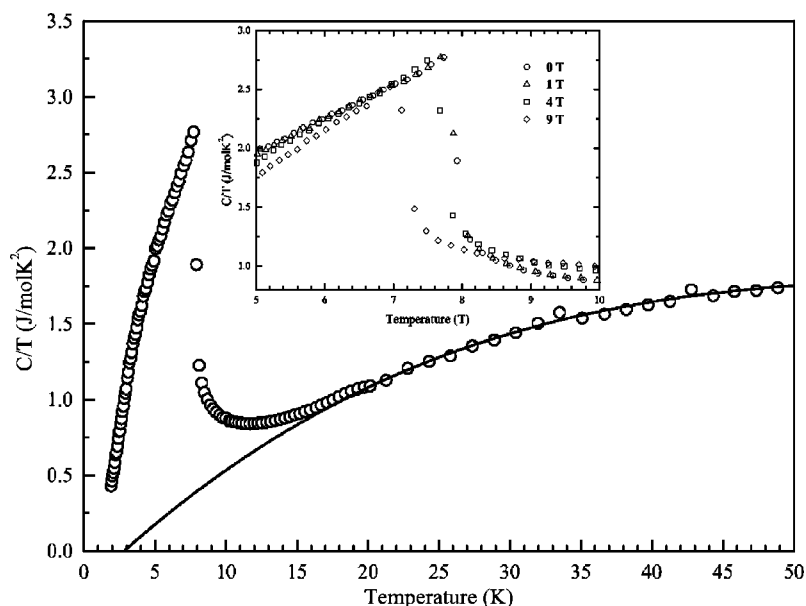
FIG. 5. Temperature dependence of the total specific heat measured at 0 T. The inset shows the variation of the total specific heat as a function of the temperature at different magnetic field strengths. The solid line represents the calculated electronic and lattice contributions to the total specific heat.

$S_{mag} = \int (C_{mag}/T)dT$. This integration has been done by fitting the C_{mag}/T vs T plot to a polynomial function between 50 and 10 K and to an exponential function between 2 and 9 K. The temperature dependence of S_{mag} is given in Fig. 6. This magnetic entropy takes the value of 10 J mol^{-1} K^{-1} in the paramagnetic state and shows a sudden decrease around 8 K, associated with the onset of the antiferromagnetic state. The magnetic entropy value for this low-temperature antiferromagnetic transition is lower than the theoretical value $2R \ln(2J+1)$ expected for a nonsplit ground term $^4I_{9/2}$ of the Nd^{3+}.

D. Simulation of the energy levels and associated wave functions

It is well known that the optical and magnetic properties of R-containing systems can be satisfactorily explained by accurately determined R energy levels and their associated wave functions. Wave functions of the $4f^N$ configurations in solids can be described by considering a total Hamiltonian that combines the free-ion or intraionic interactions, H_{FI}, as well as the crystal field (CF) effects arising from the influence of the surrounding charges on the $4f^N$ electrons, H_{CF}. The free-ion part can be written as[18]

$$H_{FI} = H_0 + \sum_{k=0,1,2,3} E^k e_k + \zeta_{4f} A_{SO} + \alpha L(L+1) + \beta G(G_2)$$
$$+ \gamma G(R_7) + \sum_{k=0,2,4} M^k m_k + \sum_{k=2,4,6} P^k p_k + \sum_{\lambda=2,3,4,6,7,8} T^\lambda t_\lambda$$

where H_0 stands for the spherically symmetric one-electron term of the Hamiltonian, E^k are the Racah parameters, ζ_{4f} is the spin-orbit coupling constant, e_k are the angular parts of the electrostatic repulsion, and A_{SO} represents the spin-orbit coupling. The Trees parameters $\alpha, \beta,$ and γ and Judd parameters T^λ, for configurations having more than two electrons,
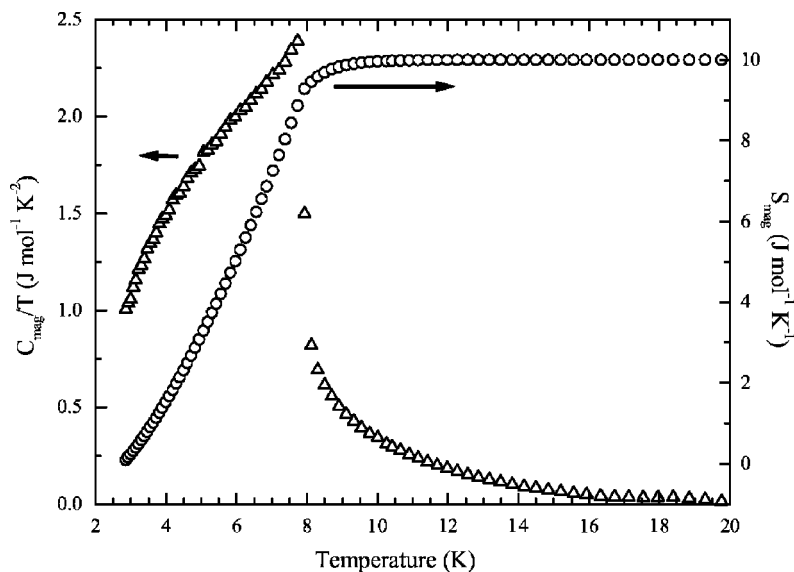
FIG. 6. Temperature dependence of the magnetic specific heat C_{mag} and magnetic entropy S_{mag} obtained from the total specific heat measured at 0 T.

account for the two- and three-body terms for the configuration interactions, respectively. Magnetically correlated corrections such as spin-spin and spin-other-orbit interactions can be simulated through the M^k parameters, also called Marvin integrals. Finally, the electrostatically correlated spin-orbit interactions are described by the P^k integrals.

Following the Wybourne formalism,[19] the one-electron H_{CF} Hamiltonian is expressed as a sum of products of spherical harmonics and real B_q^k and complex S_q^k crystal field parameters (CFPs)

$$H_{CF} = \sum_{k=2}^{4,6} \sum_{q=0}^{k} \{B_q^k[C_q^k + (-1)^q C_{-q}^k] + iS_q^k[C_q^k - (-1)^q C_{-q}^k]\}.$$

The number of the nonzero B_q^k and S_q^k phenomenological CFPs depends on the crystallographic point-site symmetry of the R ion. For the C_{2v} symmetry of the Nd^{3+} site in Nd_2BaCuO_5, the serial development of the CF potential involves nine real B_q^k CFPs. Previously,[11] closeness with the local environment of Nd^{3+} in transparent Nd_2BaZnO_5 was claimed, and consequently the expectation of similar CF interactions allows a parallel CF description of the obviously more scarce spectroscopic data in magnetic Nd_2BaCuO_5.

The analysis of the optical data, derived from nonpolarized low-temperature optical absorption and photoluminescence measurements[11] in polycrystalline samples of Nd_2BaZnO_5, for the current low-point-group symmetry requires a large number of adjustable parameters, and the result of a search for the minimum in a fitting procedure, that is, the best collection of phenomenological parameters obtained from a least-squares refinement between observed and calculated Nd^{3+} energy levels,[20] is affected by uncertainty, which results from the absence of knowledge of the irreducible representation of each level, leading to their ambiguous assignment. Various theoretical models of the CF interactions[21,22] can be used to provide convenient sets of CFPs to be compared with the above ones, alleviating this difficulty. Moreover, the consistency and reliability of the fitted parameters can be checked through simultaneous simulations performed for different $4f^N$ configurations,[18] either in the same or in an isostructural crystalline matrix, since derived CFPs should compare well, presenting only regular variations along an isostructural series. Apart from Nd_2BaZnO_5, CF analyses have not been performed for other tetragonal R_2BaZnO_5 or R_2BaCuO_5 compounds, and therefore formerly available[11] adjusted phenomenological CFPs are expected to be somewhat dubious, especially as they are overly far from calculated semiempirical CFPs. Now, we have performed a different simulation of CF interactions using the same reported[11] experimental collection of energy levels for Nd_2BaCuO_5. Starting CFPs for the fit were obtained by applying the usually successful semiempirical simple overlap model (SOM),[23] while starting free-ion parameters were maintained at the reported values.[11] The results of this fit, which includes the $^2H2_{11/2}$ energy levels and uses the reduced matrix element $\langle ^2H2_{11/2}|U^4|^2H2_{11/2}\rangle$ divided by 4,[24] are shown in Table IV. Although final mean square deviations σ are similar for both the earlier[11] and current CF fits, a better reproduction of the experimental $^4I_{9/2}$ ground state energy levels 0, 67, 228,

TABLE IV. Phenomenological free-ion and CF parameters (cm^{-1}) for Nd^{3+} in Nd_2BaZnO_5. Energy levels reported in Ref. 11 were used in the fit. Values in parentheses refer to estimated standard deviations in the indicated parameter. Values in square brackets were fixed in the parameter fitting. Italic characters indicate semiempirical SOM calculated CF parameters.

			Ref. 11
E^0		23288 (1)	23313
E^1		4910 (1)	4886
E^2		22.77 (2)	22.71
E^3		475.72 (9)	474.03
α		22.30 (4)	20.47
β		−768(4)	−702
γ		[750]	[750]
ζ		869.5 (8)	868.8
$T2$		[266]	[275]
$T3$		63 (3)	78
$T4$		52 (3)	61
$T6$		−271(6)	−278
$T7$		260 (7)	262
$T8$		[265]	240
$M^{0\,a}$		1.65 (8)	1.73
$P^{2\,b}$		197 (16)	286
B_0^2	−645	−480(21)	481
B_2^2	−437	213 (13)	44
B_0^4	−1055	−1336(44)	843
B_2^4	−1386	−1641(24)	534
B_4^4	280	35 (49)	1734
B_0^6	107	720 (43)	966
B_2^6	775	104 (38)	180
B_4^6	416	270 (35)	201
B_6^6	−228	−346(48)	−7
σ^c		18.9	17.9

$^a M^0, M^2, M^4$ were constrained by the ratios $M^2 = 0.56\, M^0, M^4 = 0.32\, M^0$.
$^b P^2, P^4, P^6$ were constrained by the ratios $P^4 = 0.75 P^2, P^6 = 0.50 P^2$.
$^c \sigma = [\Sigma(\Delta_i)^2/(l-p)]^{1/2}, \Delta_i = E_0 - E_c, l$ number of levels, p number of parameters.

287, and 460 cm^{-1} is found from our CF analysis, 0, 66, 245, 300 and 466 cm^{-1}.

The validity of the compositions of both sets of wave functions for the energy levels of Nd^{3+} in $R_2BaCuO_5(R_2BaZnO_5)$ will be checked through the comparison of calculated paramagnetic susceptibilities χ as a function of the temperature with corresponding measurements in an oriented single crystal of Nd_2BaCuO_5.

E. Paramagnetic susceptibility simulations from crystal field effects

The determination of a consistent set of energy levels for $R_2BaCuO_5(R_2BaZnO_5)$, which gives the expression of their associated wave functions, allows the calculation of χ vs T

and the ground state g values of Nd^{3+}, in the current CF environment. This is done using the Van Vleck formalism[25]

$$\chi_i = N\beta^2 \sum_a \left[\frac{\langle\varphi_a|(L+g_eS)u|\varphi_a\rangle^2}{kT} - 2\sum_b \frac{\langle\varphi_a|(L+g_eS)u|\varphi_b\rangle\langle\varphi_b|(L+g_eS)u|\varphi_a\rangle}{E_a - E_b} \right]B_a,$$

where N is Avogadro's number, β the Bohr magneton, k the Boltzmann constant, E and φ the energy levels and wave functions, unperturbed by the magnetic field respectively, described in the $|SLM_J\rangle$ basis, and $L+g_eS$ the component (i) of the magnetic interaction associated with a tensorial operator of rank 1, where the magnetic dipole operator g_e is the gyromagnetic ratio (2.0023), u being the unitary vector corresponding to the i axis. The sums run over thermally populated levels, according to the thermal partition law $B_a = \exp(-E_a/kT)/\Sigma_a \exp(-E_a/kT)$. The different values of the tensor components, or combinations of them, destroy the isotropy observed for the free ion or even for an ion in a cubic symmetry. The anisotropy components are called $\chi_\parallel$ (component 0 of the tensor) and $\chi_\perp$ (components ± 1 of the tensor). In that expression the matrix elements are calculated using the Racah algebra rules.

The formula is the sum of a temperature-dependent diagonal term and a temperature-independent off-diagonal term, which is reminiscent of the classical Curie-Weiss law. The off-diagonal term, a result of the second order perturbation, usually has little importance, with the exception of the ground states with $J=0$. The sum runs over all other states ($b \neq a$). Energy levels up to 5000 and 10 000 cm^{-1}, for the diagonal and off-diagonal terms, respectively, which are largely sufficient to cover the thermal population effect above 300 K, were accounted for in the calculation along with the J mixing of the levels.

The χ_x, χ_y, and χ_z values with respect to the orthorhombic C_{2v} point-site symmetry of Nd^{3+} in the crystal host have also been calculated with the reel program, on the basis of the wave functions from the C_{2v} CF and free-ion parameters of Table IV. Taking into account that the symmetry of Nd^{3+} has a twofold axis and a mirror plane in the equivalent directions $[1\bar{1}0]$ and $[110]$, the measured magnetic susceptibility $\chi_\parallel$ will be perpendicular to the above symmetry axis of the Nd^{3+} site, and thus it corresponds to the calculated magnetic susceptibility along the x or y direction around the point site. Conversely, the measured magnetic susceptibility $\chi_\perp$ will correspond to either $(\chi_y+\chi_z)/2$ or $(\chi_x+\chi_z)/2$ calculated paramagnetic susceptibilities. Looking upon the shape of the calculated magnetic susceptibility curves, it is clear that $\chi_\parallel$ must be taken as χ_x, and then $\chi_\perp$ corresponds to $(\chi_y+\chi_z)/2$.

Magnetic susceptibility vs T curves calculated using our best-fit CF parameters reproduce quite well the experimental values, as can be observed in Fig. 7. At low temperatures the anisotropy is significant, with the susceptibility in parallel orientation to the twofold axis of the Nd^{3+} site, χ_z, stronger than that in the perpendicular directions, and especially for χ_x. Although the deviation observed between experimental and calculated curves is obviously ascribed to the incertitude
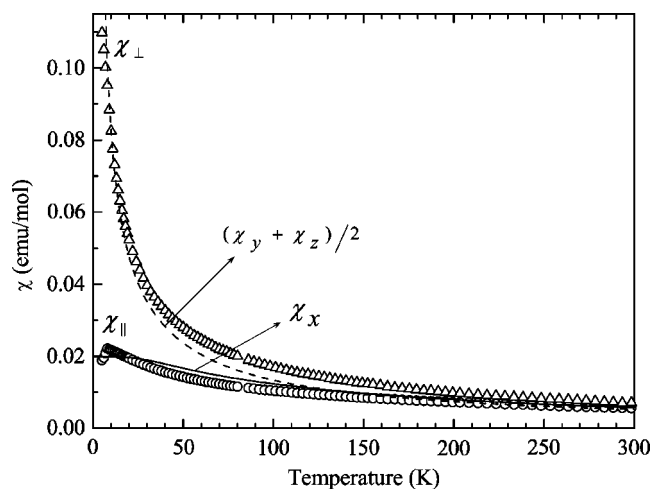
FIG. 7. Magnetic susceptibility per Nd^{3+} versus temperature for single-crystal Nd_2BaCuO_5 oxide. The triangles and circles correspond to the magnetic susceptibility per Nd^{3+} measured along the a and the c axis, respectively. The solid, and dashed lines correspond to the calculated magnetic susceptibilities per Nd^{3+}, χ_x and $(\chi_y+\chi_z)/2$, respectively.

in the current determination of the CFPs, the validity and physical meaning of our set is moreover supported by the resemblance with foreseen theoretical SOM values, not attained by the previously reported data.[11] Figure 7 illustrates the comparison between experimental and calculated curves from those results, and it is clear that even trends in the χ vs T evolution are not well reproduced, with differences getting worse when the temperature decreases. Therefore, the wave functions of the ground state level currently derived can be considered as reasonably well determined, which is important for the following discussion on experimentally determined g values. The g values derived from the above fit result to be $g_x=0.001$, $g_y=-2.254$, and $g_z=3.138$, reflecting the indicated large anisotropy.

The value of $0.81\mu_B$ obtained for antiferromagnetically ordered Nd^{3+} ions from neutron diffraction studies,[13] which is significantly smaller than the theoretical one expected of $g_J \times J = 4.20\mu_B$, can be thus explained by considering the g values derived from the crystal field simulation discussed above. According to the magnetic structure, the Nd^{3+} tends to align its magnetic moment in the ab plane, which means that the c axis constitutes a hard direction, and accordingly, the g-tensor value calculated from the crystal field simulation in the ab plane takes a value of $2.2\mu_B$, and the magnetic moment, given as $\mu(Nd^{3+})=\frac{1}{2}g_J\mu_B$, results as $1.1\mu_B$, which agrees well with that obtained from neutron diffraction experiments. Neutron experiments on single crystals are now in progress in order to get more insight about the magnetic structure in this oxide.

ACKNOWLEDGMENT

[1] A. Salinas, J. L. García, J. Rodríguez-Carvajal, R. Sáez Puche, and J. L. Martínez, J. Solid State Chem. **100**, 201 (1992).

[2] H. K. Muller-Buschbaum, and C. Lang, J. Less-Common Met. **L1**, 142 (1988).

[3] T. Chattopodhgay, P. J. Brown, U. Kobler, and E. Wihelm Europhys. Lett. **8**, 685 (1989).

[4] I. V. Golosovsky, V. P. Plakhty, V. P. Hauchenhov, J. Zoulkova, B. V. Mill, M. Bonnet, and E. Roudeau, Sov. Phys. Solid State, **34**(5), 782 (1992).

[5] A. Salinas Sánchez, R. Sáez Puche, and M. A. Alario, J. Solid State Chem. **89**, 361 (1990).

[6] F. Mizuno, H. Masuda, I. Hirabayashi, S. Tanaka, M. Hasegawa, and U. Mizutani, Nature (London) **345**, 788 (1990).

[7] H. Masuda, F. Mizuno, I. Hirabayashi, and S. Tanaka, Phys. Rev. B **43**, 7871 (1991).

[8] S. Feldkemper, W. Weber, J. Schulenburg, and J. Richter, Phys. Rev. B **52**, 313 (1995).

[9] J. B. Goodenough, *Magnetism and the Chemical Bond* (Robert Krieger, New York, 1976).

[10] R. Sáez-Puche, S. R. Herrera, and J. L. Martínez, J. Alloys Compd. **269**, 57 (1998).

[11] S. A. Klimin, M. N. Popova, E. Antic-Fidancev, and P. Porcher, J. Solid State Chem. **162**, 42 (2001).

[12] I. V. Paukov, M. N. Popova, and B. V. Mill, Phys. Lett. A **157**, 306 (1991).

[13] I. V. Golosovsky, P. Boni, and P. Fischer, Phys. Lett. A **182**, 161 (1993).

[14] A. Salinas-Sánchez and R. Sáez Puche, Solid State Ionics **63-65**, 927 (1993).

[15] H. Nozaki, H. Ikuta, Y. Yamada, A. Matsushita, H. Takahashi, I. Hirabayashi, and U. Mizutani, Phys. Rev. B **62**, 9555 (2000).

[16] *Computer code* REEL (Siemens Energy & Automation Inc., Analytical Instrumentation, 1996).

[17] C. Cascales, R. Sáez Puche, and P. Porcher, J. Solid State Chem. **114**, 52 (1995).

[18] W. T. Carnall, G. L. Goodman, K. Rajnak, and R. S. Rana, J. Chem. Phys. **90**, 3443 (1989).

[19] B. G. Wybourne, *Spectroscopic Properties of Rare Earths* (Wiley, New York, 1965).

[20] P. Porcher, *Computer code* REEL (1989).

[21] D. Garcia and M. Faucher, in *Handbook on the Physics and Chemistry of Rare Earths*, edited by K. A. Gschneidner, Jr., and L. Eyring (North-Holland, Amsterdam, 1995), Vol. 2, p. 263, and references cited therein.

[22] O. L. Malta, Chem. Phys. Lett. **88**, 353 (1982).

[23] M. Faucher, D. Garcia, E. Antic-Fidancev, and M. Lemaitre Blaise, J. Phys. Chem. Solids **50**, 1227 (1989).

[24] P. Porcher, M. Couto dos Santos, and O. Malta, Phys. Chem. Chem. Phys. **1**, 397 (1999).

[25] J. H. Van Vleck, J. Appl. Phys. **39**, 365 (1968).